Pressure tuning of the thermal conductance of weak interfaces

Wen-Pin Hsieh,[1,2,*] Austin S. Lyons,[3,4] Eric Pop,[3,4,5] Pawel Keblinski,[6] and David G. Cahill[2,7]

[1]*Department of Physics, University of Illinois, Urbana, Illinois 61801, USA*

[2]*Frederick-Seitz Materials Research Laboratory, University of Illinois, Urbana, Illinois 61801, USA*

[3]*Micro and Nanotechnology Lab, University of Illinois, Urbana, Illinois 61801, USA*

[4]*Department of Electrical and Computer Engineering, University of Illinois, Urbana, Illinois 61801, USA*

[5]*Beckman Institute, University of Illinois, Urbana, Illinois 61801, USA*

[6]*Department of Materials Science and Engineering, Rensselaer Polytechnic Institute, Troy, New York 12180, USA*

[7]*Department of Materials Science and Engineering, University of Illinois, Urbana, Illinois 61801, USA*

We use high pressure to reveal the dependence of interfacial heat transport on the stiffness of interfacial bonds. The combination of time-domain thermoreflectance and SiC anvil techniques is used to measure the pressure-dependent thermal conductance $G(P)$ of clean and modified Al/SiC interfaces at pressures as high as $P = 12$ GPa. We create low-stiffness, van der Waals–bonded interfaces by transferring a monolayer of graphene onto the SiC surface before depositing the Al film. For such weak interfaces, $G(P)$ initially increases approximately linearly with P. At high pressures, $P > 8$ GPa, the thermal conductance of these weak interfaces approaches the high values characteristic of strongly bonded, clean interfaces.

PACS number(s): 66.70.−f, 68.60.Dv

I. INTRODUCTION

Heat transport across interfaces is characterized by the interface thermal conductance G, defined by $J = G\Delta T$, where J is the heat flux and ΔT is the temperature drop at the interface. The interface thermal conductance plays a critical role in controlling thermal conduction in nanostructures,[1] nanoscale composites,[2,3] and superlattices.[4] For example, a high density of interfaces can reduce the effective thermal conductivity of materials below the amorphous limit[5,6] and therefore may find applications in improving thermoelectric energy conversion.[7]

The acoustic mismatch model (AMM) and diffuse mismatch model (DMM) are often used to predict and interpret the interface thermal conductance G.[8,9] These models assume that G is a consequence of only the lattice dynamics of the bulk materials on each side of the interface; changes in the bonding and vibrational density of states of atoms adjacent to the interface are not explicitly accounted for in these models. In the AMM, the phonon transmission at the interface is derived from differences in acoustic impedances, i.e., products of the mass density and speeds of sound. The larger the mismatch in acoustic impedance, the smaller the value of G. The DMM, on the other hand, assumes that strong phonon scattering occurs at the interface and that phonon transmission is controlled by the phonon densities of states in the materials on either side of the interface. In the DMM, the more dissimilar the densities of phonon vibrational states, the lower the value of G.

The effects of interface bonding on interface thermal transport[10–16] have been discussed for many years. For example, enhanced interface bonding between Pb and diamond was considered as a mechanism leading to the anomalously high thermal conductance of Pb/diamond interfaces.[14] Young and Maris[15] used a computational lattice-dynamics model to show that phonon transmission at an interface is reduced when the force constant of the bonds connecting atoms on the two sides of the interface is smaller than the force constants acting between atoms within the bulk of the materials on the two sides of the interface. Also using a lattice-dynamics theory,

Pettersson and Mahan showed that, due to weakened interface bonding, the thermal conductance of dissimilar lattices is lower than when the lattices match.[16] Recent molecular dynamics simulations have confirmed that low interface stiffness can significantly suppress thermal transport.[10,11] Analytical approaches[12,13] have also been developed to include the effects of weak interface bonding. In these models, in the limit of extremely weak interfaces, G scales with the square of the interface force constant; at high interface stiffness, G saturates at the value predicted by the AMM.

The interface stiffness S relates an applied stress τ to the discontinuity in displacement Δu that is generated by that applied stress, $\tau = S\Delta u$.[17] In general, the interface stiffness has normal S_L and transverse S_T components corresponding to the normal and shear components of the stress, although we do not distinguish between S_L and S_T here. If the interface is diffuse on the atomic scale, i.e., if the interface is not abrupt, then the interface stiffness can be defined by the excess displacement at the interface in a manner similar to how surface excess quantities are defined in surface thermodynamics.

High-pressure environments enable continuous tuning of the lattice dynamics of materials through the anharmonicity of atomic or molecular bonds.[18] In the experiments described here, high pressure allows us to systematically vary the interface stiffness S and directly observe the role of weak interface bonding on the suppression of thermal conductance G. By analogy with the elastic constants of materials, we expect S of a weak interface to increase linearly with pressure P with the functional form $S(P) = S_0 + S_1 P$. Anvil cell techniques[19,20] can easily generate the high pressures, typically $P \sim 10$ GPa, needed to increase the small force constants characteristic of van der Waals interactions to values more typical of strong chemical or ionic bonds.[21]

II. EXPERIMENTAL DETAILS

We prepared three types of interfaces that span the range from strong to weak: (1) a clean Al/SiC interface,

(2) Al deposited on the native oxide of SiC, and (3) a similar interface containing a monolayer of graphene, i.e., Al/graphene/SiO$_x$/SiC. The first type of interface, the clean interface, was prepared by placing a SiC anvil in a small, shallow hole drilled in a thin graphite plate and subsequently electrically heating the graphite plate to $\approx$1300 K for 30 min at a pressure of $\approx$5$\times$10^{-7} torr. The temperature of the graphite heater was measured by optical pyrometry. After allowing the SiC anvil to cool to near room temperature, an 80-nm-thick Al film was deposited *in situ* by magnetron sputtering without exposing the sample to air.

We deposited an 80-nm-thick Al film on the native oxide of the as-received SiC anvil at room temperature to form an Al/SiO$_x$/SiC interface of the second type mentioned previously. The thickness of the native oxide on the as-received SiC anvil, $\approx$1 nm, was determined by the ratio $R \approx 3$ of the integrated intensities of Si-C to Si-O peaks in the Si 2p x-ray photoelectron spectrum.[22] (The photoelectron current was measured at normal incidence.)

We also studied "weak" interfaces of the third type, which incorporate a monolayer of graphene between the Al and the native oxide layer on SiC. Monolayer graphene was first grown on a Cu foil by chemical vapor deposition (CVD).[23] We then spin coated a 250-nm-thick poly(methyl methacrylate) (PMMA) layer on one side of the Cu foil, etched the other side of the foil in an O$_2$ plasma to remove the extra graphene film, and etched the Cu foil in aqueous ferric chloride.[23] The PMMA and graphene were rinsed in deionized water and transferred to the SiC anvil. After the PMMA carrier layer was removed using a 1:1 methylene chloride/methanol solution, the sample was annealed at $\approx$670 K for 1 h at atmospheric pressure using a gas flow of 500 sccm of H$_2$ and 500 sccm of Ar to remove organic contaminants. We performed Raman spectroscopy to characterize the number of layers of the graphene transferred on the SiC anvil; the full width at half-maximum (FWHM) of the 2D peak of graphene, $\approx$34 cm^{-1}, confirms that the graphene is monolayer.[24] (Bilayer graphene is easily distinguished from monolayer graphene by a significantly larger FWHM of $\approx$60 cm^{-1}.[24])

We prepared two variants of weak type (3) interface samples. For the first one, we transferred the CVD-grown graphene directly to the as-received SiC anvil, as described previously. We also prepared a second variant of the sample to test the dependence of the thermal conductance on the thickness of the native oxide layer. For this second sample, the as-received SiC was first cleaned at high temperatures as described previously and then exposed to ambient air for $\approx$24 h. X-ray photoelectron spectroscopy data showed that the thickness of the regrown native oxide layer was $\approx$0.5 nm. For both weak interface samples, the graphene-covered SiC anvil was heated to $\approx$420 K to remove volatile contaminants before depositing Al.

We pressurized the SiC anvil cells by loading the cell with Ar or H$_2$O as the pressure medium. The pressure was determined by ruby fluorescence.[25] The thermal conductance G of Al/SiC interfaces was measured by comparing time-domain thermoreflectance (TDTR)[1,26,27] data obtained at room temperature with calculations using a thermal model that takes into account the heat flow through the interface layer and into the SiC substrate, as well as the heat flow

into the pressure medium.[28–31] The thermal model contains several parameters—laser spot size ($w_0 \approx 6.5\ \mu$m) and the thickness, heat capacity, and thermal conductivity of each layer—but the thermal conductance of Al/SiC interfaces is the only significant unknown. The thickness of the Al film h_{Al} at ambient pressure was determined for each sample by picosecond acoustics.[32] We calculated the changes in h_{Al} under pressure by assuming that the Al film adheres well to the SiC anvil surface and that the Al film deforms plastically;[33] h_{Al} decreases by 5.4% at 5 GPa and 9.4% at 10 GPa. Our estimate of the pressure dependence of the volumetric heat capacity of Al is described in Ref. [20]. For an 80-nm-thick Al film, the heat capacity per unit area is $h_{Al}C = 1.94\times10^{-5}$ J cm^{-2} K^{-1} at ambient conditions and decreases by 4% at 10 GPa.

III. RESULTS AND DISCUSSION

Example TDTR data for type (2) Al/SiO$_x$/SiC interfaces and fits to the thermal model are shown in Fig. 1. The ratio V_{in}/V_{out} decreases faster as the applied pressure increases, indicating that the interface thermal conductance increases with pressure. The overall uncertainty in the measurements of G is $<$8% and is dominated by the uncertainty in the thickness of the Al film. In our sample geometry, most of the heat deposited by each pump optical pulse flows into the high thermal conductivity SiC anvil and only a small fraction of the heat flows into the low thermal conductivity pressure medium; consequently, the results are relatively insensitive to the thermal conductivity and heat capacity of the pressure medium and uncertainties in these thermal properties propagate to less than an $\approx$2% error in G.

Figure 2(a) shows the pressure dependence of the thermal conductance $G(P)$ of the various Al/SiC interfaces we have studied. The thermal conductance of the clean Al/SiC interface (open circles) at ambient pressure is high, $G \approx 200$ MWm^{-2} K^{-1}, and is weakly dependent on pressure. (The thermal conductance of interfaces in Al/SiC metal–matrix composites was previously found to be $G \approx 150$ MWm^{-2} K^{-1} using thermal conductivity measurements as a function of SiC particle size and analysis of the data
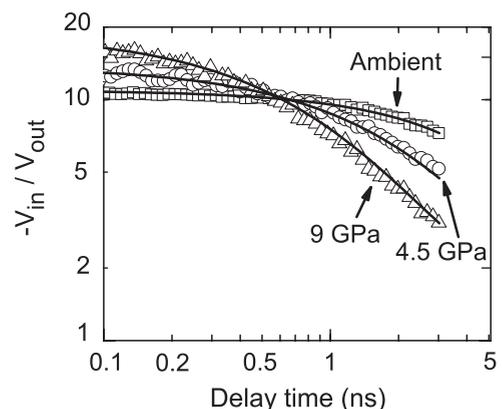
FIG. 1. Example data (open symbols) for TDTR measurements on Al/SiO$_x$/SiC interfaces and fits (solid lines) to the thermal model as described in Refs. [28–31]. Data and fits are labeled by the pressure. The interface thermal conductance is enhanced by the increasing pressure.
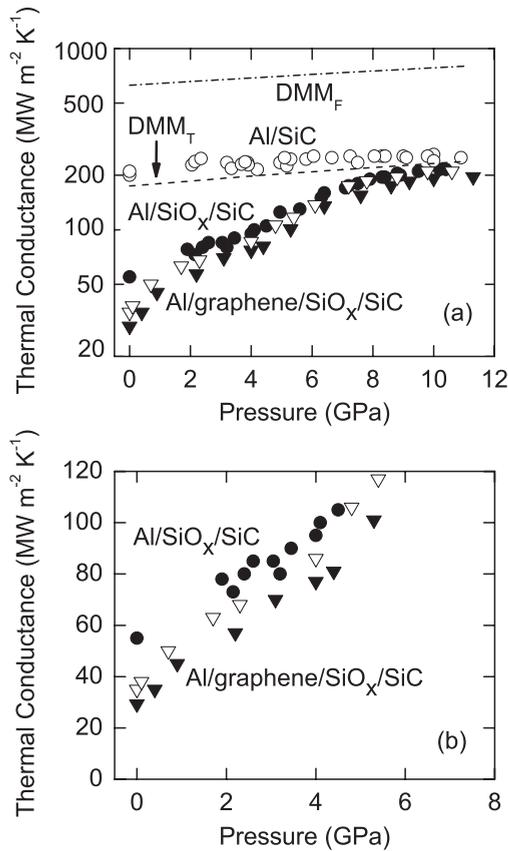
FIG. 2. (a) Pressure dependence of the thermal conductance $G(P)$ of various Al/SiC interfaces. $G(P)$ of the clean Al/SiC interface (open circles) is weakly dependent on the pressure. By contrast, $G(P)$ of the weak interfaces Al/SiO$_x$/SiC (solid circles) and Al/graphene/SiO$_x$/SiC (open and solid triangles) increases rapidly with pressure due to the increasing interface stiffness and approaches the value of the clean Al/SiC interface at $P > 8$ GPa. The thickness of the native oxide on SiC for solid triangle data, ≈ 1 nm, is twice as thick as that for the open triangle data, ≈ 0.5 nm. The DMM prediction of $G(P)$ of the Al/SiC interface is shown as the dashed line for the truncated model (DMM$_T$) and as a dashed-dot line for the full Debye model (DMM$_F$). (b) $G(P)$ of weak interfaces in the low pressure regime. The symbols for each interface are the same as in (a).

by effective medium theory.[34]) This result is consistent with our assumption that deposition of Al on clean SiC creates a strongly bonded interface with high interface stiffness.

We compare our data for $G(P)$ to the predictions of two versions of the DMM: a calculation using a full Debye phonon density of states (DMM$_F$); and a calculation in which the Debye density of states is truncated at the frequencies of the zone boundary phonons (DMM$_T$). An illustration of these models is given in Fig. 3. In both calculations, we allow conversion of the polarization of phonon modes at the interface. The full Debye model typically overestimates the DMM interface conductance near room temperature because the reduction of the phonon group velocity at high wavevectors is not taken into account; this reduction in phonon group velocity suppresses contributions to the interface conductance from high-wavevector phonons.[35,36] The truncated model is similar to that described in Ref. 37 in that we assume linear
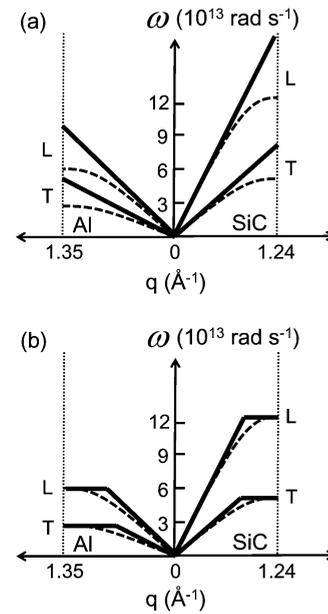
FIG. 3. Illustration of the acoustic phonon dispersions in Al in the [111] direction and in SiC in the [0001] direction. (a) The full Debye model (DMM$_F$) assumes linear phonon dispersions (solid lines) across the Brillouin zone. (b) In the truncated Debye model (DMM$_T$), the phonon dispersions (solid lines) are assumed to be linear and truncated at cutoff frequencies determined by the frequencies of each phonon mode at the zone boundary. An illustration of the experimental phonon dispersions in Al and SiC are shown as dashed curves. L and T denote the longitudinal and transverse modes, respectively.

phonon dispersions in Al and SiC and set the longitudinal and transverse cutoff frequencies using the frequencies of each acoustic phonon mode at the Brillouin zone boundary in the [111] direction for Al[38] and [0001] direction for SiC.[39] We also assume that the pressure dependence of the cutoff frequencies scales with the Debye frequencies of Al and SiC at high pressures. The truncated model underestimates the DMM interface conductance because contributions to heat transport by short-wavelength phonons are omitted. Thus, we believe that these two model calculations, DMM$_F$ and DMM$_T$, would bracket the DMM conductance that would be calculated if phonon dispersion could be taken into account accurately.

The experimental results for the clean type (1) Al/SiC lie slightly above the DMM$_T$ calculation and are a factor of ≈ 3 smaller than the DMM$_F$ calculation at all pressures [Fig. 2(a)]. The pressure dependence of the data is also similar to the pressure dependence predicted by the models. The calculated $G(P)$ using DMM$_T$ has a rate of change with pressure, $dG/dP \approx 6$ MW m^{-2} K^{-1} GPa^{-1}, that agrees closely with the experimental average slope for the clean Al/SiC interface, $dG/dP \approx 4.5 \pm 1$ MWm^{-2} K^{-1} GPa^{-1}.

Also shown in Fig. 2(a) are data for the type (2) Al/SiO$_x$/SiC interface, which shows strikingly different behavior. At ambient pressure, $G \approx 55$ MW m^{-2} K^{-1}, a factor of 4 smaller than G of a clean Al/SiC interface. Moreover, $G(P)$ of the Al/SiO$_x$/SiC interface increases dramatically with pressure before approaching the value of a clean Al/SiC interface ≈ 200 MWm^{-2} K^{-1} at $P > 8$ GPa. We attribute such behavior of $G(P)$ of the weak Al/SiO$_x$/SiC interface to low

interface stiffness at low pressure that strongly suppresses heat conduction at the interface.

The low thermal conductance and strong pressure dependence of the Al/SiO$_x$/SiC structure is surprising because the thermal conductance of interfaces formed by the deposition of Al on the native oxide of Si is typically >100 MW m^{-2} K^{-1}. The thermal conductivity of the native oxide of SiC would have to be <0.1 W m^{-1} K^{-1}, an unphysically small value for an amorphous oxide, to produce such a small conductance. We can only speculate that the interface between the native oxide of SiC and SiC itself is in some sense weakly bound, perhaps due to the formation of carbonaceous layers at the interface.[40]

To examine the behavior when the interface stiffness is reduced further, we now turn to the type (3) samples described previously, with a layer of graphene inserted at the Al/SiO$_x$ interface. The inclusion of graphene at the interface decreases G at ambient pressure by an additional factor of ≈2. The open triangles in Fig. 2 are $G(P)$ of Al/graphene/SiO$_x$/SiC with a 0.5-nm-thick native oxide layer grown on precleaned SiC, and the solid triangles are $G(P)$ of Al/graphene/SiO$_x$/SiC with the 1-nm native oxide layer of the as-received SiC anvil. The data for the 1-nm oxide layer are slightly lower than the data for the 0.5-nm oxide layer over the entire range of pressure, indicating that the thicker oxide layer creates a small additional thermal resistance.

The addition of graphene to the interface affects the thermal conductance compared to the Al/SiO$_x$/SiC sample but only at lower pressures of $P < 6$ GPa. We attribute this observation to weak van der Waals bonding at graphene interfaces and, consequently, the low stiffness of the Al/graphene/SiO$_x$ interface. As the low stiffness of the van der Waals bonding increases with pressure and becomes comparable to the stiffness of the Al/SiO$_x$/SiC structure, the effect of the inserted graphene layer on the thermal conductance becomes insignificant.

Data for $G(P)$ shown in Fig. 2 include measurements for both increasing and decreasing P. The lack of any obvious hysteresis shows that changes in the interface stiffness under pressure are reversible.

At $P < 6$ GPa, $G(P)$ of weak interfaces increases approximately linearly with pressure with a functional form $G(P) = G_0 + G_1 P$ [Fig. 2(b)]. The data for $G(P)$ approach the values for the clean Al/SiC interface at $P > 8$ GPa. The overall behavior of $G(P)$ is consistent with the results of molecular dynamics simulations on qualitatively similar interfaces.[10,11] We point out, however, that the phenomenological linear relationship between G and P in the low pressure regime is not a simple consequence of the linear increase in interface stiffness S with pressure. Increasing pressure causes S to increase and a higher value of S increases the characteristic frequency that separates low-frequency phonons with high transmission coefficients from high-frequency phonons with low transmission coefficients.[41] Therefore, as the stiffness increases, the average phonon transmission coefficient increases and eventually approaches a large value when the majority of the distribution of heat-carrying phonons is able to scatter at the interface.

Pressure tuning of the interface bonding over a broad range of stiffness demonstrates that interface stiffness dominates the thermal transport at weak interfaces but plays a minor role for strong interfaces. An analytical treatment of a simple one-dimensional model of two semi-infinite chains of masses connected by springs and forming a point junction demonstrated that the transmission coefficient of phonons dominating thermal transport is approximately proportional to the interface force constant and saturates when the interface springs are of similar stiffness to the stiffness of bonds in the bulk of the materials.[41]

*whsieh2@illinois.edu

[1] D. G. Cahill, W. K. Ford, K. E. Goodson, G. D. Mahan, A. Majumdar, H. J. Maris, R. Merlin, and S. R. Phillpot, J. Appl. Phys. **93**, 793 (2003).

[2] C. W. Nan, R. Birringer, D. R. Clarke, and H. Gleiter, J. Appl. Phys. **81**, 6692 (1997).

[3] S. Shenogin, L. P. Xue, R. Ozisik, P. Keblinski, and D. G. Cahill, J. Appl. Phys. **95**, 8136 (2004).

[4] Y. K. Koh, Y. Cao, D. G. Cahill, and D. Jena, Adv. Funct. Mater. **19**, 610 (2009).

[5] C. Chiritescu, D. G. Cahill, N. Nguyen, D. Johnson, A. Bodapati, P. Keblinski, and P. Zschack, Science **315**, 351 (2007).

[6] R. M. Costescu, D. G. Cahill, F. H. Fabreguette, Z. A. Sechrist, and S. M. George, Science **303**, 989 (2004).

[7] S. T. Huxtable, A. R. Abramson, C. L. Tien, A. Majumdar, C. LaBounty, X. Fan, G. H. Zeng, J. E. Bowers, A. Shakouri, and E. T. Croke, Appl. Phys. Lett. **80**, 1737 (2002).

[8] E. T. Swartz and R. O. Pohl, Rev. Mod. Phys. **61**, 605 (1989).

[9] A. Janzen, B. Krenzer, P. Zhou, D. von der Linde, and M. H. V. Hoegen, Surf. Sci. **600**, 4094 (2006).

[10] M. Hu, P. Keblinski, and P. K. Schelling, Phys. Rev. B **79**, 104305 (2009).

[11] Z. Y. Ong and E. Pop, Phys. Rev. B **81**, 155408 (2010).

[12] B. N. J. Persson, A. I. Volokitin, and H. Ueba, J. Phys. Conden. Matt. **23**, 045009 (2011).

[13] R. Prasher, Appl. Phys. Lett. **94**, 041905 (2009).

[14] R. J. Stoner and H. J. Maris, Phys. Rev. B **48**, 16373 (1993).

[15] D. A. Young and H. J. Maris, Phys. Rev. B **40**, 3685 (1989).

[16] S. Pettersson and G. D. Mahan, Phys. Rev. B **42**, 7386 (1990).

[17] P. Nagy, J. Nondestr. Eval. **11**, 127 (1992).

[18] R. G. Ross, P. Andersson, B. Sundqvist, and G. Backstrom, Rep. Prog. Phys. **47**, 1347 (1984).

[19] P. Beck, A. F. Goncharov, V. V. Struzhkin, B. Militzer, H. K. Mao, and R. J. Hemley, Appl. Phys. Lett. **91**, 181914 (2007).

[20]W. P. Hsieh, B. Chen, J. Li, P. Keblinski, and D. G. Cahill, Phys. Rev. B **80**, 180302 (2009).

[21]W. P. Hsieh, M. D. Losego, P. V. Braun, S. Shenogin, P. Keblinski, and D. G. Cahill, Phys. Rev. B **83**, 174205 (2011).

[22]C. Onneby and C. G. Pantano, J. Vac. Sci. Tech. A **15**, 1597 (1997).

[23]J. D. Wood, S. W. Schmucker, A. S. Lyons, E. Pop, J. W. Lyding, Nano Lett. (2011), doi: 10.1021/nl201566c.

[24]D. Graf, F. Molitor, K. Ensslin, C. Stampfer, A. Jungen, C. Hierold, and L. Wirtz, Nano Lett. **7**, 238 (2007).

[25]H. K. Mao, P. M. Bell, J. W. Shaner, and D. J. Steinberg, J. Appl. Phys. **49**, 3276 (1978).

[26]C. A. Paddock and G. L. Eesley, J. Appl. Phys. **60**, 285 (1986).

[27]D. A. Young, C. Thomsen, H. T. Grahn, H. J. Maris, and J. Tauc, in *Phonon Scattering in Condensed Matter*, edited by A. C. Anderson and J. P. Wolfe (Springer, Berlin, 1986), p. 49.

[28]Z. B. Ge, D. G. Cahill, and P. V. Braun, Phys. Rev. Lett. **96**, 186101 (2006).

[29]D. G. Cahill, Rev. Sci. Instrum. **75**, 5119 (2004).

[30]A. Schmidt, M. Chiesa, X. Y. Chen, and G. Chen, Rev. Sci. Instrum. **79**, 064902 (2008).

[31]P. E. Hopkins, B. Kaehr, L. M. Phinney, T. P. Koehler, A. M. Grillet, D. Dunphy, F. Garcia, and C. J. Brinker, J. Heat Trans. **133**, 061601 (2011).

[32]C. Thomsen, H. T. Grahn, H. J. Maris, and J. Tauc, Phys. Rev. B **34**, 4129 (1986).

[33]B. Chen, W. P. Hsieh, D. G. Cahill, D. R. Trinkle, and J. Li, Phys. Rev. B **83**, 132301 (2011).

[34]D. P. H. Hasselman, K. Y. Donaldson, and A. L. Geiger, J. Am. Ceram. Soc. **75**, 3137 (1992).

[35]P. Reddy, K. Castelino, and A. Majumdar, Appl. Phys. Lett. **87**, 211908 (2005).

[36]J. C. Duda, T. E. Beechem, J. L. Smoyer, P. M. Norris, and P. E. Hopkins, J. Appl. Phys. **108**, 073515 (2010).

[37]Y. K. Koh, M. H. Bae, D. G. Cahill, and E. Pop, Nano Lett. **10**, 4363 (2010).

[38]R. Stedman and G. Nilsson, Phys. Rev. **145**, 492 (1966).

[39]D. W. Feldman, J. H. Parker, W. J. Choyke, and L. Patrick, Phys. Rev. **173**, 787 (1968).

[40]G. V. Soares, C. Radtke, I. J. R. Baumvol, and F. C. Stedile, Appl. Phys. Lett. **88**, 041901 (2006).

[41]L. F. Zhang, P. Keblinski, J. S. Wang, and B. W. Li, Phys. Rev. B **83**, 064303 (2011).